Available online at www.sciencedirect.com

ScienceDirect

Procedia Engineering 00 (2016) 000–000

Procedia Engineering

www.elsevier.com/locate/procedia

1st International Conference on the Material Point Method, MPM 2017

# MPM simulations of the interaction between water jet and soil bed

Dongfang Liang[a,*], Xuanyu Zhao[a,b], Mario Martinelli[b]

[a]*Department of Engineering, University of Cambridge, Trumpington Street, Cambridege CB2 1NX, UK*
[b]*Deltares, Boussinesqweg 1, 2629 HV Delft, The Netherlands*

**Abstract**

In offshore engineering, pipelines are often buried in the seabed to avoid the damage caused by ocean waves, currents, fishing activities, *etc*. For its reliability, the high-speed water jet has been increasingly used for constructing the pipe trenches. The jet-soil interaction is a highly complicated two-phase problem. A three-dimensional Material Point Method (MPM) model, Anura3D (www.anura3d.com), is used to simulate the jet trenching processes. In this preliminary study, the effect of the water jet speed on the trenching process is simulated. The research demonstrates the advantages of the MPM model in handling the free surface and soil-water interaction problems, and the results are useful for the offshore oil and gas industry. In future research, the different controlling parameters of the trenching operation, including the jet size, water pressure, translational speed and soil strength, will be tested to optimize the trenching operation to achieve high efficiency.

Peer-review under responsibility of the organizing committee of the 1 st International Conference on the Material Point Method.

*Keywords:* material point method; pipeline trench; two-phase flow; soil-water interaction; erosion; scour.

## 1. Introduction

The erosion of bed soil with traveling high-speed water jets has wide engineering usage. In offshore oil and gas industry, this technique is often used to construct the trenches on the seabed for burying subsea pipelines. The subsea pipeline is an important part of the oil and gas exploration. It could convey the oil or gas conveniently from the well to the storage and onshore factories. More and more pipelines are being laid on the sea bed. For the purpose of protecting the pipeline from damage of wave impact and fishing trawls, the pipes should be buried beneath the seabed at 1 m – 3 m depth. Most of those trenches are constructed using the jet trencher, for its reliability [1]. The

* Corresponding author.
*E-mail address:* d.liang@eng.cam.ac.uk


Peer-review under responsibility of the organizing committee of the 1 st International Conference on the Material Point Method.

mechanism of jet-soil interaction is very complex, so the jet trench depth prediction remains a challenge in the jet trencher design.

The modern mesh-free computational techniques offer new opportunities for predicting the dynamic soil-water interaction problems. In particular, the Material Point Method (MPM) makes use of both discrete Lagrangian interpolation points and Eulerian mesh in the computation [2]. The motion of Lagrangian interpolation points are tracked throughout the computation. Its origin is the Arbitrary Lagrangian-Eulerian method (ALE) [3], the Particle in cell (PIC) method [4], the Fluid Implicit Particle (FLIP) method [5] and the Finite Element Method (FEM) [6]. MPM has many attractive advantages over traditional numerical methods, and is becoming increasingly popular in simulating various solid mechanics problems with large deformation. Firstly, it is convenient to use with history-dependent constitutive models because state variables, such as strain and stress, are carried by material points, which enables the spatial and temporal tracking of these history-dependent variables. Secondly, the use of a background mesh allows for the implementation of boundary conditions in a manner similar to that in FEM, whereas many other mesh-free methods often find it challenging to incorporate the accurate boundary conditions. Many mesh-free methods suffer from unphysical particle clumping or even particle penetration when particles are under tensile stress state, but MPM effectively avoids such tensile instability by retaining the background mesh in the computation [7]. At the beginning of each time step, all the data required for solving the governing equations are mapped from the particles to the neighbouring grid nodes. Then, the weak form of the governing equations is solved at the grid nodes and this solution is used to update the material points. In both FLIP and MPM, the governing equations for the fluid flow are solved on the Eulerian grid and the particle variables are updated in accordance with the grid-based solutions. A key difference of the two methods is that MPM solves the weak formulation of the governing equations, so the MPM is presented in the same framework as FEM. In addition, the constitutive equations are invoked at the material points in MPM whereas in FLIP they are solved at the grid nodes [8].

The current MPM techniques for simulating soil-water interactions generally fall into two categories: one uses a single set of material points [9-11] and the other uses two sets of material points [12-14]. Bandara & Soga [15] and Martinelli [16] gave a detailed literature review concerning different numerical techniques and pointed out the merits and shortcomings of each application. The single particle methods assume similar velocities of the soil skeleton and pore water. In reality, the pore water moves relative to soil skeleton, thus the true water velocity is different from water velocity of the soil material point computed from the formulation with only a single set of material points. It is necessary to consider the motion of the water phase by considering either the true velocity field or relative water velocity with respect to soil skeleton. The paper demonstrates the application of a dual-particle MPM model to the impact of high-speed water jets on the soil bed.

## 2. Dual-particle MPM model

The two sets of material points represent solid skeleton and water, respectively, and they are allowed to occupy the same location. There are two sets of primary unknowns to be determined. Hence, the behavior of the dry soil, pure water and saturated soil can be modelled in a unified framework. In this formulation, the momentum conservative equations are solved to obtain the acceleration of the solid skeleton and the fluid phase separately. Momentum exchange term (or interaction force) is considered in terms of the drag force. Where water and soil particles coexist in an element, Terzaghi's effective stress concept is adopted for the soil skeleton unless the soil grains are fluidised, in which case the intergranular force becomes zero and the soil particles move under the action of the submerged weight and drag force only.

In the following, the quantities associated to the solid phase and liquid phase are referred with *S* and *W*, respectively, in the subscripts. The momentum conservation equations are:

$$(1-n)\rho_S \frac{D\mathbf{u}_S}{Dt} = \nabla \cdot \bar{\boldsymbol{\sigma}}_S + (1-n)\rho_S \mathbf{g} + \mathbf{f}_d \tag{1}$$

$$n\rho_W \frac{D\mathbf{u}_W}{Dt} = \nabla \cdot \bar{\boldsymbol{\sigma}}_W + n\rho_W \mathbf{g} - \mathbf{f}_d \tag{2}$$

where $t$ is time, $D/Dt$ is the material derivative; $n$ is the porosity, $\rho$ is density, $\mathbf{u}$ is velocity vector, $\boldsymbol{\sigma}$ is the Cauchy stress tensor, $\mathbf{g}$ is the gravitational acceleration, and $\mathbf{f}_d$ accounts for the coupling drag force between water flow and soil skeleton. It should be noted that the macroscopic partial stresses, indicated by an overbar, are used that are defined over the specific area of the mixture, but the intrinsic velocities are used in the above governing equations. The stress of the soil material is linked to the soil constitutive model. The liquid material is assumed to be weakly compressible, whose mean stress (pressure) is determined by the liquid bulk modulus $K$ and volumetric strain (density) whereas the deviatoric stress tensor is determined by the fluid viscosity coefficient $\mu$ and shear strain rate tensor.

The drag force is composed of two contributions [17]:

$$\mathbf{f}_d = n^2\left(\frac{\mu}{k} + n\rho_W \frac{F}{\sqrt{k}}\left|\mathbf{u}_W - \mathbf{u}_S\right|\right)\left(\mathbf{u}_W - \mathbf{u}_S\right) - p_W \nabla n \tag{3}$$

The Ergun's law for the drag force is used, where $k$ is the soil intrinsic permeability given by Bear [18], $F$ is a coefficient and $p_W$ is the intrinsic water pressure (the isotropic part of $\boldsymbol{\sigma}_W = \overline{\boldsymbol{\sigma}}_W / n$).

$$k = \frac{d^2}{A}\frac{n^3}{(1-n)^2} \tag{4}$$

$$F = \frac{B}{A^{1/2} n^{3/2}} \tag{5}$$

$d$ is the effective grain size, $A$ is set to 150 and $B$ is set to 1.75 [19].

The total stress can also be partitioned into effective stress $\boldsymbol{\sigma}_S$' and liquid stress, the latter of which can be taken as the intrinsic partial stress of the liquid constituent:

$$\overline{\boldsymbol{\sigma}}_S + \overline{\boldsymbol{\sigma}}_W = \overline{\boldsymbol{\sigma}}_S + n\boldsymbol{\sigma}_W = \boldsymbol{\sigma}_S' + \boldsymbol{\sigma}_W \tag{6}$$

Hence, the macroscopic stress on the solid phase is:

$$\overline{\boldsymbol{\sigma}}_S = \boldsymbol{\sigma}_S' + (1-n)\boldsymbol{\sigma}_W \tag{7}$$

Equations (1-2) can then be written into:

$$(1-n)\rho_S \frac{D\mathbf{u}_S}{Dt} = \nabla \cdot \boldsymbol{\sigma}_S' + (1-n)\nabla \cdot \boldsymbol{\sigma}_W + (1-n)\rho_S \mathbf{g} + \mathbf{f}_d \tag{8}$$

$$n\rho_W \frac{D\mathbf{u}_W}{Dt} = n\nabla \cdot \boldsymbol{\sigma}_W + n\rho_W \mathbf{g} - \mathbf{f}_d \tag{9}$$

The conservation of mass leads to the following equations for the solid and liquid constituents:

$$\frac{D\overline{\rho}_S}{Dt} + \overline{\rho}_S \nabla \cdot \mathbf{u}_S = 0 \tag{10}$$

$$\frac{D\overline{\rho}_W}{Dt} + \overline{\rho}_W \nabla \cdot \mathbf{u}_W = 0 \tag{11}$$

Assuming the intrinsic density of the solid to be constant, the change in the macroscopic density is due to the change in porosity which can be related to the stress condition of the soil. From these two equations, the density (volumetric strain) of the liquid can be obtained [16]:

$$\frac{1}{\rho_W}\frac{D\rho_W}{Dt} = \frac{1}{n}\left[(1-n)\nabla\cdot\mathbf{u}_S + n\nabla\cdot\mathbf{u}_W + \nabla n\cdot(\mathbf{u}_W - \mathbf{u}_S)\right] \tag{12}$$

which can be used to determine the water pressure.

An important judgement in the present formulation is the state of the solid-liquid mixture, which can also be carried out by monitoring the local porosity of the soil. If the local porosity is low, then the grains are in contact and the behavior of the mixture can be described by various constitutive models in soil mechanics. Conversely, if the local porosity is very high, the collection of soil grains becomes loose with no contact force among one another. Then, the effective stresses are set to zero and the mixture is fluidised. In all the following simulations, the threshold porosity for judging the state of the soil-water mixture has been taken to be 0.5, as labelled in Table 1 in the next section.

## 3. Simulation of the interaction between water jet and soil bed

### *3.1. Numerical model setup*

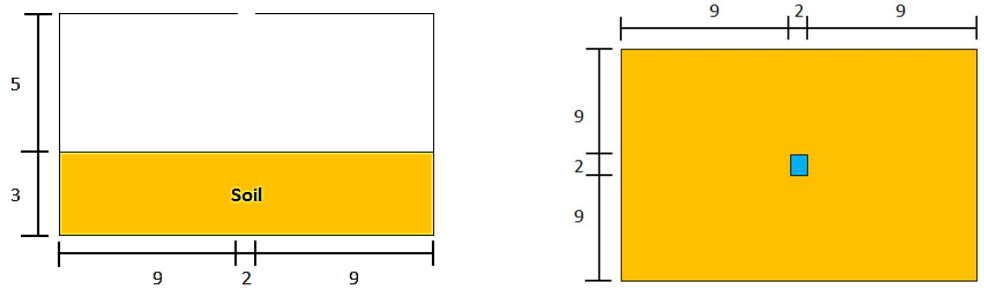


Fig. 1. Computational domain: (left) side view; (right) top view.

Table 1. Computational parameters.

| Computational parameter | Value |
|---|---|
| Solid grain diameter | 0.258 mm |
| Density of soil grains | 2650 kg/m$^3$ |
| Young's modulus of soil | 10000 kPa |
| Poisson ratio of soil | 0.3 |
| Friction angle | 30 degree |
| Dilatancy angle | 5 degree |
| Initial porosity | 0.43 |
| Maximum porosity | 0.5 |
| Water density | 1000 kg/m$^3$ |
| Water bulk modulus | 20000 kPa |
| Water viscosity | 0.001 Pa·s |

We apply the dual-particle MPM model to an idealised three-dimensional soil-water interaction problem, which involves pure water, dry soil and soil-water mixture. Fig. 1 shows the computational domain, where the labelled lengths are of the units of meters. The soil bed has dimensions of 20 m in length, 20 m in width and 3 m in depth. In this preliminary study, the cross section of the water jet is taken to be a square with a side length of 2 m. The inlet of the water jet is 5 m above the soil bed. Water particles are supplied from the inlet with different velocities to study the sensitivity of the trenching operation to the water jet speed. The values of the key computational parameters are listed in Table 1. The bulk modulus of water was assigned an unrealistically low value, so that a relatively large time step could be specified in the simulation. Such a strategy is commonly used in many mesh-free methods. As long as the modelled water has a sound speed over 10 times larger than the maximum flow velocity, the increased compressibility of water does not affect the results much [20].

In this preliminary study, only sandy soil is considered and the standard Mohr-Coulomb model is taken as the soil constitutive model. Around 21,000 tetrahedral elements are used to discretize the domain, with an average side length of around 1 m. Initially, 20 solid material points are deployed per element in the soil layer. In specifying the inlet boundary condition, we also assume that on average 20 water particles are needed to fill up an element near the inlet boundary. The soil and water particles are allowed to co-exist in an element, as is the essence of the dual-particle MPM model.

### *3.2. Simulation results*

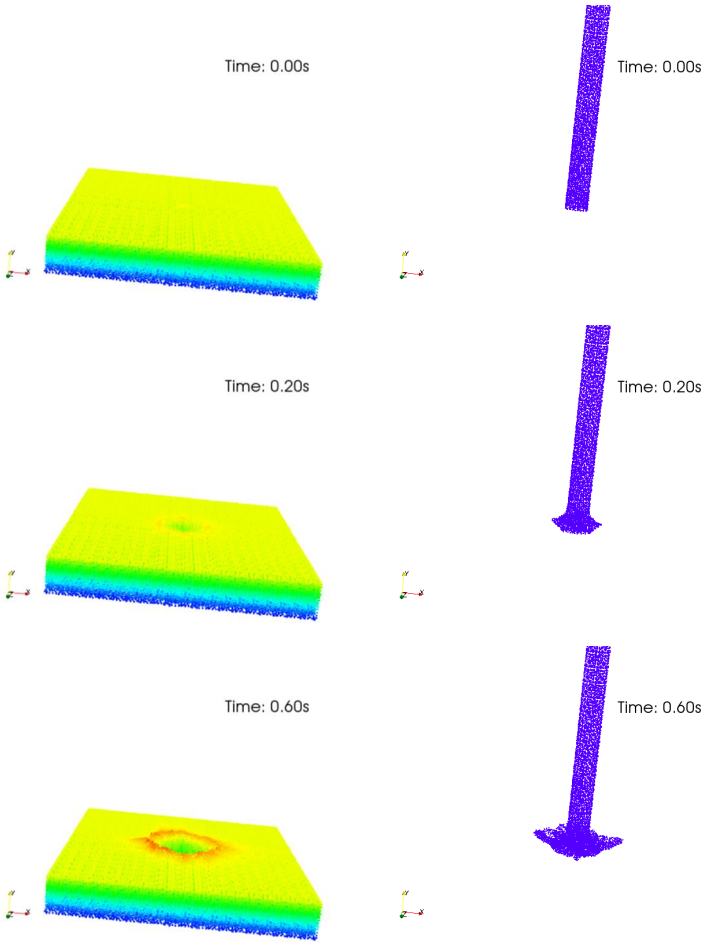

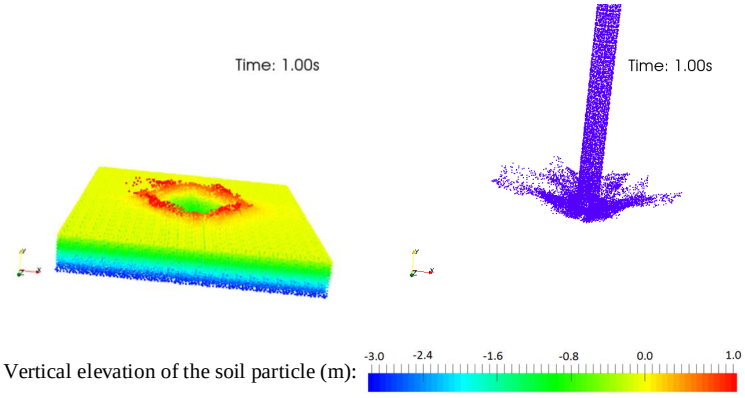


Fig. 2. Evolution of the shapes of the soil bed and water jet, with a jet speed of 17 m/s.

The interaction of the high-speed water jet and the soil bed is illustrated by the evolution of the soil and water shapes in Figs. 2-4. The three different jet speeds were chosen to be within the range of the recent experiment on subsea jet trenchers [21]. In order to effectively visualise the shape of the scoured pit on the bed, the vertical elevations of the soil particles are highlighted with different colours. The datum of the vertical elevation is the initial horizontal bed, so the elevation of the bottom of the soil layer is -3 m. The failure of the soil bed under the impact of high-speed water jet can be reasonably reproduced by the MPM model. As the jet speed increases, the displacement of the soil particles also increases. Corresponding to the increased degree of soil deformation, the water jet becomes increasingly scattered on smashing on the soil bed.

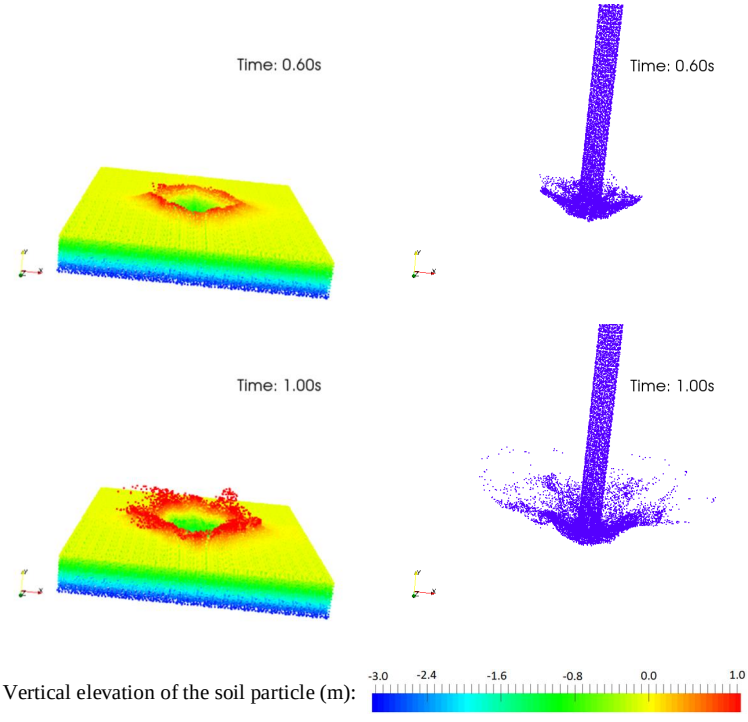


Fig. 3. Evolution of the shapes of the soil bed and water jet, with a jet speed of 22 m/s.

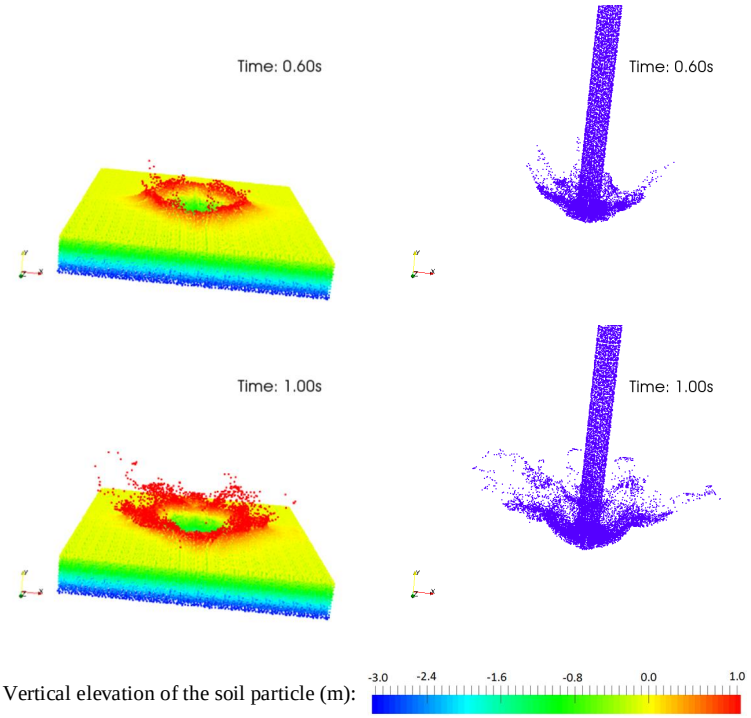


Fig. 4. Evolution of the shapes of the soil bed and water jet, with a jet speed of 27 m/s.

The depth of the impact pit in the soil layer, along the centreline of the jet, is used as an indicator of the soil bed deformation. The interface of water and soil is reconstructed based on the distribution of the discrete solid particles. Fig. 5 summarises the development of the impact pit's depth with time. As can be seen, the impact pit deepens with time almost linearly in the first 1 second. As expected, the impact pit is deeper with the higher speed of the water jet.

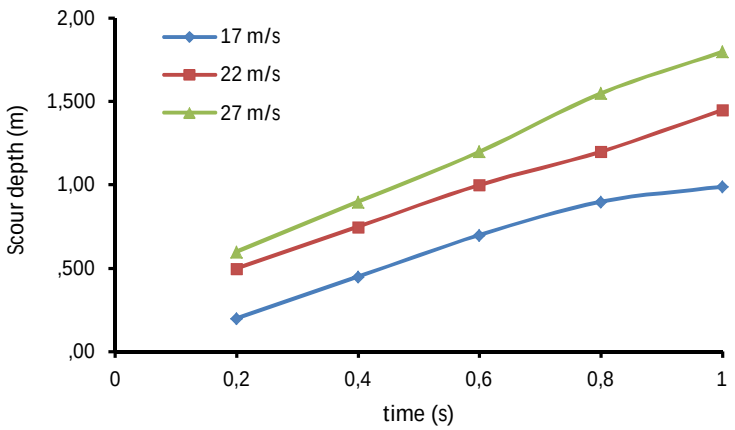


Fig. 5. Development of the scour depth with time.

## 4. Conclusions

The general principle of a dual-point MPM model is introduced in this paper. Because the two sets of material points are allowed to move separately, such a model is suitable for simulating problems involving large relative velocities between the solid skeleton and water. The dual-point MPM model (Anura3D) has been applied to model the interaction of a high-speed water jet and a soil bed, and the results are encouraging. The preliminary study illustrates the capability of the present MPM model, but it does not fully reflect the realistic trenching process of the water jet. The key factors of the jet trenching operation include the shear strength of soil, water jet velocity, nozzle diameter and the translational speed of nozzle. We will consider the travelling of the water jet in the horizontal direction, and will quantitatively compare the simulations with the experimental data in the near future.

## Acknowledgements

We acknowledge the financial support of the MPM-DREDGE Project funded by the European Commission's Seventh Framework Programme (PIAP-GA-2012-324522), and the National Natural Science Foundation of China (Grant Nos. 51541911 and 51479111).

## References

[1] F.D. Messina, J.B. Machin, J.F. Hill, The economic advantages of jet-assisted plowing, OCEANS 2001, MTS/IEEE Conference and Exhibition 1 (2001) 649-652.
[2] L. Moresi, F. Dufour, H.B. Mühlhaus, A Lagrangian integration point finite element method for large deformation modeling of viscoelastic geomaterials, Journal of computational physics 184 (2003) 476–497.
[3] C.W. Hirt, A.A. Amsden, J.L. Cook, An arbitrary Lagrangian-Eulerian computing method for all flow speeds, Journal of computational physics 14 (1974) 227-253.
[4] F.H. Harlow, A machine calculation method for hydrodynamic problems, Los Alamos Scientific Laboratory report, LAMS-1956.
[5] J.U. Brackbill, D.B. Kothe, H.M. Ruppel, FLIP: a low-sissipation, particle-in-cell method for fluid flow, Computational physics communications 48 (1988) 25-38
[6] O.C. Zienkiewicz, R.L. Taylor, J.Z. Zhu, The finite element method: its basis and fundamentals (6th edition), Butterworth-Heinemann, Oxford.
[7] S. Ma, X. Zhang, X.M. Qiu, Comparison study of MPM and SPH in modeling hypervelocity impact problems, International journal of impact engineering 36 (2009) 272–282.
[8] D. Sulsky, Z. Chen, H.L. Schreyer, A particle method for history-dependent materials, Computer methods in applied mechanics and engineering 118 (1994) 179–196.
[9] H.W. Zhang, K.P. Wang, Z. Chen, Material point method for dynamic analysis of saturated porous media under external contact/impact of solid bodies, Computer methods in applied mechanics and engineering 198 (2009) 1456–1472.
[10] I. Jassim, D. Stolle, P. Vermeer, Two-phase dynamic analysis by material point method, International journal for numerical and analytical methods in geomechanics 37 (2013) 2502–2522.
[11] E.E. Alonso, F. Zabala, Progressive failure of Aznalcóllar dam using the material point method, Géotechnique 61 (2011) 795–808
[12] C. Li, R.I. Borja, R.A. Regueiro, Dynamics of porous media at finite strain, Computer methods in applied mechanics and engineering 193 (2004) 3837–3870.
[13] W.K. Shin, Numerical simulations of landslides and debris flows using an en-hanced material point method, University of Washington, 2009.
[14] P. Mackenzie-Helnwein, P. Arduino, W. Shin, J.A. Moore, G.R. Miller, Modeling strategies for multiphase drag interactions using the material point method, International journal for numerical methods in engineering 83 (2010) 295–322.
[15] S. Bandara, K. Soga, Coupling of soil deformation and pore fluid flow using Material Point Method, Computers and geotechnics 63 (2015) 199–214.
[16] M. Martinelli, Soil-water interaction with material point method, MPM Research Community Report, Deltares, Delft, Netherlands, 2016.
[17] I. Vardulakis I, Fluidisation in artesian flow conditions: Hydromechanically stable granular media, Geotechnique 54 (2004) 117-130.
[18] J. Bear, Dynamics of fluids in porous media. Elsevier, Amsterdam, 1972.
[19] S. Ergun, Fluid flow through packed columns, Chemical engineering progress 48 (1952) 89-94.
[20] D. Liang, Evaluating shallow water assumptions in dam-break flows, Proceedings of the institution of civil engineers – water management 163 (2010) 227-237.
[21] S. Zhang, The research of subsea jet trencher's jetting system and application, PhD thesis, Shanghai Jiao Tong University, 2015.